Circulation in Bubble Columns

L. F. Burns and R. G. Rice
Dept. of Chemical Engineering, Louisiana State University, Baton Rouge, LA 70803

Liquid circulation in bubble columns influences many system properties such as mass transfer and catalyst dispersion. Conditions favorable for liquid circulation often exist only for highly turbulent slurries. Experiments under conditions of lowered surface tension proved conclusively that uniform circulation can exist even in the bubbly-flow regime. Moreover, the measured circulating velocity profile is more plug-shaped in the center core than traditional models, which take a parabolic shape. These observations led to the application of a circulation theory based on an energy-dissipation model for turbulent eddy viscosity, which can be easily computed as a simple function of superficial-gas velocity. Two length scales were used in model calculations depending on flow regime: bubble diameter for bubbly flow and column diameter for churn turbulence. The liquid-velocity profile contained a tuned dimensionless proportionality constant, which resulted in two different average values, $k = 2.51$ for bubbly flow and 0.0242 for churn turbulence, when tuned to experimental data. The integral average eddy viscosity is numerically equivalent to the eddy dispersion coefficient for bubbly flow. Predicted liquid velocity compared very favorably with new measured values under conditions of low surface tension and with literature values.

Introduction

Bubble-column design is most often concerned with the transfer of mass between phases either for separation or to supply reactants to a liquid-phase reaction. In either case, *a priori* knowledge of the mass-transfer characteristics is required for design. However, it is well known that mass exchange is primarily determined by the global hydrodynamics present in the bubble column (Shah et al., 1982; Rice et al., 1993). This has been typically represented by correlations based on system and physical properties. Although useful, these correlations do little to elucidate the link between mass transfer and the overall hydrodynamics on which they are founded. Moreover, they do not explain the effect of the induced liquid circulation patterns on mass transfer.

Attempts have recently been made using turbulent properties, such as Reynolds stresses, to explain the liquid hydrodynamics from a fundamental standpoint (Rice and Geary, 1990; Geary and Rice, 1992; Menzel et al., 1990; Luo and Svendsen, 1991). These attempts have been somewhat successful, but the fundamental turbulent parameters, such as Prandtl's length scale and eddy viscosity, have been primarily based on single-phase turbulence data. Experimental liquid circulation profiles found in the literature often exhibit plug-shaped profiles in the center of the column rather than parabolic, as suggested by the predicted values (Hills, 1974; Menzel et al., 1990; Ueyama and Miyauchi, 1979). Moreover, this problem is confounded by the lack of reliable liquid velocity data to test new velocity prediction theories. Another problem is the lack of detailed information on the system studied with a few notable exceptions (Devanathan et al., 1990, 1995; Hills, 1974, 1976; Menzel et al., 1990; Rietema and Ottengraf, 1970; Ulbrecht and Baykara, 1981; Ueyama and Miyauchi, 1979).

Considering the successful dispersion model of Baird and Rice (1975), a new turbulent (eddy) viscosity is introduced containing an arbitrary proportionality constant, k. This allows, for the first time, a simple calculation of local turbulent viscosity as a function of superficial gas velocity and a length scale. The velocity profile may be expressed as a simple algebraic function of this single parameter, k. This parameter was tuned to literature velocity data in both the bubbly-flow and churn-turbulent flow regimes. The predicted velocity profiles not only fit the data well, but also matched the pluglike shape of the data in the central core of the column. Most other velocity-prediction models, especially those based on single-phase turbulence data, yield profiles that are parabolic in shape. The present model is compared to liquid-circulation

Correspondence concerning this article should be addressed to R. G. Rice.
Current address of L. F. Burns: Exxon Research and Development Laboratories, Baton Rouge, LA 70805.

data obtained in surfactant-laced aqueous solutions using an innovative combination of two well-known velocity measurement techniques.

During the course of investigating velocity profiles in bubble columns, a fascinating phenomenon was discovered. Intense, global liquid circulation was observed when small amounts of surfactant were added to an aqueous bubble column. This was surprising, since the bubble column was operating well within the bubbly-flow regime ($U_{OG} \approx 2$ cm/s), which normally does not sustain circulation. Bubbly flow and churn turbulence are used throughout this work in the context defined by Wallis (1969). Simply stated, bubbly flow occurs under low superficial gas velocities less than 4 cm/s, while churn turbulence occurs at gas velocities higher than for bubbly flow. It manifests itself by the onset of periodic churning and slug formation. When operating under virtually identical conditions, liquid circulation was not observed for tap-water systems. This unexpected response to the surfactant has not heretofore appeared in the literature. Moreover, the bubble column used in this study was installed to be perfectly vertical, using the spring-micrometer system described elsewhere (Rice et al., 1990). True verticality has a profound effect in reducing liquid circulation and dispersion in the bubbly-flow regime (Rice and Littlefield, 1987). Tilted columns sustain liquid upflow on the downfacing wall and downflow on the other, even for bubbly-flow conditions. Columns that are slightly tilted often have mixing times that are almost an order of magnitude less than one aligned perfectly vertical (Rice et al., 1990).

Following initial mixing-time experiments, we set out to measure the local interstitial liquid velocity profile under conditions of intense circulation. Both the Pavlov-tube method and hot-wire anemometry measurement techniques encountered separate, but significant difficulties in the surfactant laced (contaminated) system. Later in this article, we will present an innovative method of coupling the two-measurement techniques to successfully measure velocity profiles in contaminated systems. The results of these experiments further indicate that the velocity profiles are plug shaped in the center of the column rather than parabolic.

Essence of the Model

The liquid circulation patterns, given as axial liquid-velocity profiles, depend on and are in fact driven by variations in the radial distribution of the local gas holdup (Anderson and Rice, 1989; Deckwer et al., 1974; Geary and Rice, 1992; Hills, 1974; Luo and Svendsen, 1991; Menzel et al., 1990). The exact nature of the radial distribution appears to take the form of a polynomial of varying degree as suggested by several authors (Rice and Geary, 1990; Ueyama and Miyauchi, 1979). Rice and Geary (1990) modified the polynomial of Ueyama and Miyauchi (1979) by introducing λ, so that a bubble-free zone exists when $\xi > \lambda$:

$$\epsilon(\xi) = \bar{\epsilon}\frac{m+2}{m}\left(1-\left(\frac{\xi}{\lambda}\right)^m\right). \qquad (1)$$

Here, ξ denotes the local dimensionless radial position, r/R, and $\bar{\epsilon}$ is the mean voidage. Several researchers fitted values

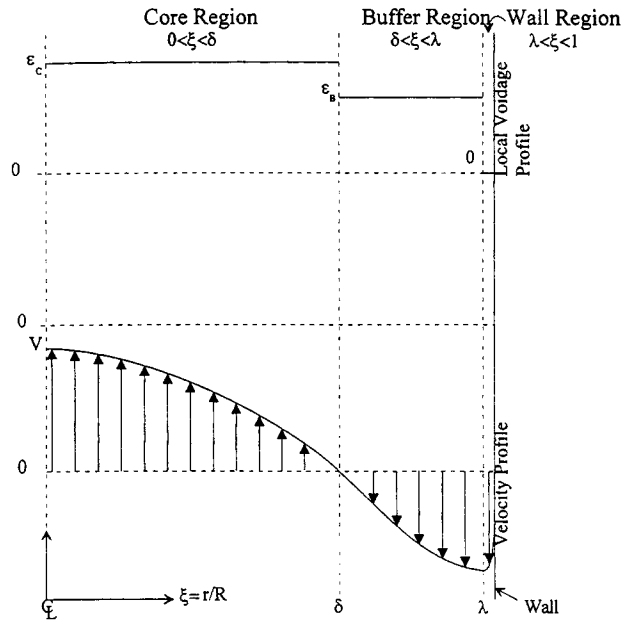

Figure 1. Three regions in a bubble column and their demarcation points.

for the power exponent m in the range 6–8 (e.g., Geary and Rice, 1992; Rice and Geary, 1990). This suggests a very flat profile in the central core.

We exploit this observation by posing a model for voidage as a staircase function. The column is apportioned into three concentric regions as seen in Figure 1: a central core, an annular buffer region, and a thin layer of clear liquid near the wall. Furthermore, the distribution of local gas hold-up is constant in each region, but varies between the regions, that is, as a staircase. The voidage in the center is higher than in the buffer region, which in turn is higher than the voidage near the wall. We take the thin wall region to be free of bubbles. The existence of the clear liquid near the wall has also been reported by the visual observations of Ulbrecht and Baykara (1981) and Rice and Geary (1990). This thin bubble-free layer may not be easily observable in low-viscosity solutions such as water. In high-viscosity liquid solutions, however, a bubble street is readily apparent. Bubbles exist and rise only in this bubble street while clear liquid exists in the remainder of the column (Rietema and Ottengraf, 1970). As depicted in Figure 1, the three regions are demarcated by δ and λ. The demarcation point δ represents the division between the central core and buffer regions (it is the zero velocity point), and the demarcation point λ represents the division between the buffer and wall regions. As will be shown later, the parameter δ and λ help characterize the shape of the velocity profiles.

The voidage profile may be related to the mean voidage by performing an integral average of the local voidage over the entire column. Since the proposed voidage profile is a simple staircase, the average may be performed easily:

$$\bar{\epsilon} = 2\int_0^{\lambda} \epsilon(\xi)\xi\, d\xi$$

$$= \epsilon_C\delta^2 + \epsilon_B(\lambda^2 - \delta^2), \qquad (2)$$

where ϵ_C is the voidage in the central core and ϵ_B is the voidage in the buffer region. Thus, we see that the mean voidage depends on four parameters. If two are measured (say $\bar{\epsilon}$ and ϵ_C), we could then find $\epsilon_B = f(\delta, \lambda)$. The preceding equation also represents the conservation of gas mass in the bubble column.

Momentum Balance

The development of momentum balances for two-phase flow is still being debated, yielding similar but slight variations to the resulting balances (Ishii, 1975; Rietema, 1982; Ishii and Zuber, 1979; Wallis, 1969). The most popular development of the equations has been formulated with the help of the "separated flow model" (Ishii, 1975; Rietema, 1982; Ishii and Zuber, 1979), which yields the following liquid (continuous-phase) and gas (dispersed-phase) momentum balances written in vector notation as

$$(1-\epsilon)\rho_L \frac{DU}{Dt} = -\nabla\cdot(1-\epsilon)\bar{\boldsymbol{T}} - (1-\epsilon)\nabla p + (1-\epsilon)\rho_L \boldsymbol{g} + \boldsymbol{F}_S \tag{3}$$

$$\epsilon\rho_g \frac{DV}{Dt} = -\nabla\cdot\epsilon\bar{\boldsymbol{T}} - \epsilon\nabla p + \epsilon\rho_g \boldsymbol{g} - \boldsymbol{F}_S. \tag{4}$$

Here, the two equations are related to one another through two fundamental variables: the value of the local gas-phase holdup (voidage), ϵ, and the slip force, $\boldsymbol{F}_S$, which represents the exchange of momentum between phases. By adding Eqs. 3 and 4 and considering only the z-directed momentum balance, the relation for the local value of the total stress becomes after some rearrangement:

$$\frac{1}{\xi}\frac{d(\xi T)}{d\xi} = \rho_L g R\left(\underbrace{\frac{-1}{\rho_L g}\frac{dp}{dz}}_{p'} - (1-\epsilon(\xi))\right), \tag{5}$$

where the dimensionless pressure gradient, p', is defined in Eq. 5. We have ignored the gravity contribution from the gas phase, which is small compared to the liquid phase.

Equation 5 applies to each of the three regions illustrated in Figure 1, and may be integrated therein subject to the following boundary conditions, $T_C(0) = 0$, $T_B(\lambda) = 0$, and $T_W(\lambda) = 0$. The subscripts represent each of the three regions. These points represent maximum and minimum of velocity where the stress tends to zero. From the boundary conditions, we can integrate Eq. 5 to give for each region:

Core region, $0 \le \xi \le \delta$:

$$T_C(\xi) = \left[\frac{\rho_L g R}{2}(p' - 1 + \epsilon_C)\right]\xi, \tag{6}$$

Buffer region, $\delta \le \xi \le \lambda$:

$$T_B(\xi) = \left[\frac{\rho_L g R}{2}(1 - \epsilon_B - p')\right]\left(\frac{\lambda^2}{\xi} - \xi\right), \tag{7}$$

Wall region, $\lambda \le \xi \le 1$:

$$T_W(\xi) = \left[\frac{\rho_L g R}{2}(1 - p')\right]\left(\frac{\lambda^2}{\xi} - \xi\right). \tag{8}$$

A simple overall force balance shows that the wall stress is

$$\tau_W = \frac{\rho_L g R}{2}(p' - 1 + \bar{\epsilon}). \tag{9}$$

The continuum stress must equal this, $T_W(1) = \tau_W$, so it must be true that

$$1 - p' = \frac{\bar{\epsilon}}{\lambda^2}, \tag{10}$$

which is identical to the relation between the pressure gradient and the mean voidage uncovered by Geary and Rice (1992) using the power-law voidage model given by Eq. 1. Note, when $p' < (1 - \bar{\epsilon}/\lambda^2)$, the force at the wall is directed downward. The expression for the dimensionless pressure gradient may now be substituted into Eqs. 6–8, yielding the stress relations in terms of the spatial coordinates and two buoyancy driving forces, $(\epsilon_C - \bar{\epsilon}/\lambda^2)$ and $(\bar{\epsilon}/\lambda^2 - \epsilon_B)$. For flat voidage profiles in which the voidages in the core and buffer region are equal (i.e., ideal bubbly flow), the two buoyancy driving forces are identically zero, and consequently the liquid does not circulate.

The total stress balances, given by Eqs. 6–8, are equal to the sum of the Newtonian stress and the Reynolds stress. Using Boussinesq's eddy-viscosity model as the Reynolds stress, the stress balance in each region must take the form

$$-\left(\frac{\mu_L + \mu_t(\xi)}{R}\right)\frac{dU}{d\xi} = T(\xi), \tag{11}$$

where the turbulent viscosity, μ_t, is a strong function of the dimensionless radial position (Bird et al., 1960). The velocity gradient may be easily solved, yielding the general expression valid for all three regions:

$$\frac{dU}{d\xi} = -\beta\frac{f(\xi)}{\frac{\nu_t(\xi)}{\nu_L} + 1}, \tag{12}$$

where $f(\xi)$ and β are defined for each of the three regions in Table 1.

Table 1. Factors for Eq. 12

	$f(\xi)$	β
Core region	ξ	$\frac{g d_C^2}{8\nu_L}\left(\epsilon_C - \frac{\bar{\epsilon}}{\lambda^2}\right)$
Buffer Region	$\frac{\lambda^2}{\xi} - \xi$	$\frac{g d_C^2}{8\nu_L}\left(\frac{\bar{\epsilon}}{\lambda^2} - \epsilon_B\right)$
Wall Region	$\frac{\lambda^2}{\xi} - \xi$	$\frac{g d_C^2}{8\nu_L}\frac{\bar{\epsilon}}{\lambda^2}$

The parameter β in Eq. 12 may be considered a measure of the capacity for liquid circulation, since it is dependent both on the buoyancy driving force and the system properties. Moreover, it is readily apparent that this capacity factor also depends strongly on both the column cross-sectional area and the liquid viscosity. As the value of β increases (by decreasing liquid viscosity, increasing column diameter, or increasing the sharpness of the voidage profile), the magnitude of liquid circulation in a bubble column is known to become more pronounced (Shah et al., 1982).

Diessler (Knudsen and Katz, 1958) proposed that the turbulent-viscosity distribution for single-phase turbulence follows the simple dimensional relation:

$$\nu_t \propto \hat{U} l, \tag{13}$$

where $\hat{U}$ and l represent the turbulent fluctuation velocity and turbulent length scale. This model is still valid in two-phase flow systems, as long as proper care is taken to select the appropriate length and velocity scales. Using axial dispersion data obtained in two-phase bubble columns, the model of Baird and Rice (1975) and Rice and Littlefield (1987) suggests that

$$\hat{U} = (P_m l)^{1/3} \tag{14}$$

where P_m is the energy dissipated in the column per unit mass and was taken to be the input energy, $U_{OG}g$. For most bubble columns operating in the churn-turbulent flow regime ($U_{OG} > 4$ cm/s), the maximum turbulence length scale for mixing is on the order of the column diameter (Baird and Rice, 1975; Devanathan et al., 1995), and accordingly, the global turbulence length, l, should scale with the column diameter, d_C, tending to zero as the wall is approached. Similarly, for columns operating in the bubbly flow regime, the global turbulence length, l, should scale with the bubble diameter (Rice and Littlefield, 1987; Rice and Geary, 1990). Circulation is normally absent in the bubbly-flow regime. For circulating bubble columns, the turbulence length scale is likely to be the column diameter (Baird and Rice, 1975). However, we produce evidence that circulation can occur in the bubbly-flow regime and the corresponding length scale may be the bubble diameter. As a first approximation, the distribution can be taken as an nth-order polynomial expression, $(1-\xi^n)$, so that the turbulence scale is at a maximum in the column center and zero at the wall. Substituting this expression for the turbulent velocity and column diameter for the length scale, Eq. 13 becomes

$$\nu_t(\xi) = k(U_{OG}g)^{1/3} d_C^{4/3} (1-\xi^n)^{4/3} \tag{15}$$

for the churn-turbulent flow regime. To account for flow in the bubbly-flow regime, it is a simple matter to replace the column diameter, d_C, with the bubble diameter, d_B, in Eq. 15. The dimensionless proportionality constant, k, and the exponent, n, define the magnitude and the shape of the eddy viscosity, respectively. We note in passing that Baird and Rice (1975) found eddy dispersion to follow $D_e = 0.35(U_{OG}g)^{1/3} d_C^{4/3}$, in the churn-turbulent regime, while Rice and Littlefield (1987) found $D_e = d_B^{4/3} (U_{OG}g)^{1/3}$ for perfectly vertical bubbly flow.

Knowing the form of the eddy viscosity, we solve for the velocity gradient in general terms as

$$\frac{dU}{d\xi} = -\alpha\beta \frac{f(\xi)}{(1-\xi^n)^{4/3} + \alpha}, \tag{16}$$

where α is the ratio:

$$\alpha = \frac{\nu_L}{k(U_{OG}g)^{1/3} d_C^{4/3}}. \tag{17}$$

For each region of the bubble column, the velocity profile is given by the integral expressions:

$$U_C(\xi) = \int_\delta^\xi \frac{dU_C}{d\xi} d\xi, \tag{18}$$

$$U_B(\xi) - U_W(\lambda) = \int_\lambda^\xi \frac{dU_B}{d\xi} d\xi, \tag{19}$$

and

$$U_W(\xi) = \int_1^\xi \frac{dU_W}{d\xi} d\xi. \tag{20}$$

However, four parameters (λ, δ, k, and n) need to be resolved before the velocity profile can be integrated.

Closure

If the proportionality constant, k, and exponent, n, are taken to be adjustable parameters that are tunable, then only two parameters need be specified. The calculation procedure is as follows. The values of k and n are assumed; the profiles are calculated; and then, the profiles are checked against the experimental data to see if a good guess was made. We use a value of $n = 2$ for the calculations. Grienberger and Hofmann (1992), using a two-dimensional k-ϵ turbulence model, found that simple parabolic profiles of the eddy viscosity were needed to fit experimental liquid-velocity data. This particular value of n considerably simplifies the analytic form of the velocity profiles, as shown in the Appendix. We note that when $n = 2$, the integral average of ν_t in Eq. 15 is such that $(\nu_t)_{avg} = 3/7\ \nu_t(0)$.

Now, only the values of the inversion point, δ, and the maximum downflow position, λ, need be determined. This requires two more constraints. The first constraint enforces continuity of the velocity at the inversion point, δ. The velocity at this point must necessarily be equal to zero whether approached from the core region or from the buffer region. By definition, the velocity in the core region is zero at this point (see Eq. 18), but the buffer region velocity defined by Eq. 19 does not necessarily go to zero at δ. Thus, the first constraint is

$$U_B(\delta) = 0 = U_W(\lambda) + \int_\lambda^\delta \frac{dU_B}{d\xi} d\xi, \tag{21}$$

which may also be written solely in terms of the velocity gradients as

$$\int_1^{\lambda} \frac{dU_W}{d\xi} d\xi + \int_{\lambda}^{\delta} \frac{dU_B}{d\xi} d\xi = 0. \quad (22)$$

The preceding constraint is only a function of δ and λ, once a value of k is specified.

The second and final constraint imposes the conservation of mass on the liquid. In the liquid-batch system considered here, the total flow of liquid must be zero. Additionally, the overall balance may be easily modified to account for cocurrent or countercurrent flow of the liquid. For a batch-liquid system in which mass exchange from the gas phase is considered negligible, the liquid mass balance may be written on a macroscale as

$$\rho_L(Q_C + Q_B + Q_W) = 0, \quad (23)$$

where Q is the volumetric liquid flowrate in each of the three respective regions. If expressed in terms of the interstitial liquid velocity, the total liquid mass balance becomes

$$2\pi R^2 \rho_L \left((1-\epsilon_C) \int_0^{\delta} U_C(\xi) \xi \, d\xi + (1-\epsilon_B) \int_{\delta}^{\lambda} U_B(\xi) \xi \, d\xi + \int_{\lambda}^{1} U_W(\xi) \xi \, d\xi \right) = 0, \quad (24)$$

which after integration by parts, leads to the final constraint in terms of the defined velocity gradients:

$$(1-\epsilon_C) \int_0^{\delta} \xi^2 \frac{dU_C}{d\xi} d\xi + (1-\epsilon_B) \int_{\delta}^{\lambda} \xi^2 \frac{dU_B}{d\xi} d\xi - \int_{\lambda}^{1} (\epsilon_B \lambda^2 - \xi^2) \frac{dU_w}{d\xi} d\xi = 0. \quad (25)$$

These final two constraints (Eqs. 22 and 25) allow implicit solutions for δ and λ. For both constraints, the velocity gradient in each of the three regions, not the velocity itself, is sufficient to close the system if a specification is made regarding the value of the final unknown parameter, k. The unknown value of the proportionality constant will be tuned to experimental data taken from literature data and also from new liquid circulation data to be presented shortly.

Some authors have opted to employ yet another constraint on the bubble column (to solve for unknown parameters), usually in the form of the energy balance (Anderson and Rice, 1989; Geary, 1992; Ishii, 1975). This yields a balance between the rate of energy input and the energy dissipation rate in the bubble column that is influenced primarily by the interaction between phases or the "slip" between the gas and the liquid. There is some contention regarding the exact form that the equations describing the interphase interaction should take (e.g., the slip force), which yields slightly different energy balances, depending primarily on the style chosen for the slip force, F_S, and energy dissipation rate (Rietema, 1982; Wallis, 1969; Ishii, 1975). In addition, several expressions for the slip force exist (see the review article by Shaw et al., 1982), which by themselves will produce some inconsistency from one energy balance to another. Geary (1992) has introduced a local drift-flux expression in place of the energy-balance equation to close his system of equations, and he found that the integral drift-flux constraint yielded slightly different but consistent results with that of the energy-balance constraint. Likewise, the integral drift-flux expression used in the comparison also required an empirical expression describing the slip between the gas and the liquid. It is interesting to note that the different formulations of the equations produce similar results; however, care must be taken in the choice of the form of the balance. Given that the energy balance equations are based on a significant level of empiricism, this balance will be discarded in favor of tuning a single parameter, k, to experimental data available both in the literature and those obtained from this work in a perfectly vertical bubble column.

Experimental Methods

Experiments to assess the voidage and liquid velocity were conducted to provide a database for comparison to velocity predictions. Because the column used in this study was perfectly aligned, a very stable bubbly-flow operating regime was produced. As such, the initial experiments with tap-water systems indicated mainly stable bubbly flow without significant circulation. Rice and Littlefield (1987) describe a technique using a visual tracer (an acid–base reaction with phenolphthalein present) to gauge column verticality. Both their column and the column used in this study were mounted on a single pivot point (a ball bearing), which could be carefully tilted in any direction with the help of a spring-loaded caliper system attached halfway up the column (see Figure 5). Adjustment to the calipers were made, while the tracer was injected into the column, to ensure a flat, plug-shaped front. Skewed tracer fronts indicated nonverticality conditions. The lowest level of axial dispersion corresponded to a "perfectly" vertical column. Details of this system are given by Rice and Littlefield (1987); Rice et al. (1990); Geary (1992); and Burns (1995). The degree of accuracy obtained relative to using a simple plumb is quite significant, with details described in Rice and Littlefield (1987). An estimate of the liquid circulation was initially gauged using these acid–base dispersion tests, which are described in the following subsection.

Acid–base method

The acid–base neutralization technique was originally designed to infer axial liquid dispersion coefficients. A concentrated base was slowly pumped into the bottom of the bubble column into a slightly acidic solution containing an indicator, phenolphthalein. As the alkali reacted with the acid, the solution changed from a clear to a bright pink color, demarcating the alkali region from the acidic region. The demarcation between the acid and alkali solutions took the form of a horizontal plane in the noncirculating, vertical bubble column with the clear acid solution above the colored alkali solution. The low level of local mixing in the bubble column tends not to disrupt this demarcation plane, also called the line of neutralization (LON), so that the LON slowly rises up the column. Even at high gas flow rates, the LON could be easily discerned and followed. This pink, alkali solution slowly ascends the column, eventually neutralizing all of the acid. By

noting the time required to completely neutralize the column, a measure of the axial liquid dispersion or backmixing can be calculated. Obviously, as the time required to fully neutralize the column becomes shorter, the level of liquid mixing becomes greater. Thus, intense circulation was not obvious from these tests owing to the exceedingly long time required to fully neutralize the column [20–30 min to neutralize ~ 7 ft (2.1 m) of gas–liquid emulsion]. Even in the churn-turbulent regime, complete liquid mixing was achieved after nearly 10 min (Burns, 1995).

However, when a small amount of surfactant, notably sodium dodecyl sulfate and decyl alcohol as an antifoaming agent, was added to the liquid during the neutralization test, obvious liquid circulation commenced almost immediately and could be visually observed. This was visualized as a sharp, upward-pointing plume of pink, phenolphthalein saturated alkali solution being "pumped" up the center of the column. The column was completely mixed in a matter of two minutes, even when using extremely low gas flow rates (rates typically characterized by the bubbly flow regime, 1.25–3 cm/s). This amounts to nearly an order-of-magnitude increase in the effective liquid dispersion coefficient. Moreover, the ordered form of the upward plume suggests an ordered flow structure as seen in the literature: liquid upflow in the center and liquid downflow near the wall.

The lowered surface-tension system provided a good opportunity to test the liquid circulation predictions, if the liquid velocity could be accurately measured, the subject of the next section. The addition of surfactant to the water produced a milky solution, which was not transparent. However, bubble size near the wall could be easily ascertained. Large variations in bubble size were not apparent in the vicinity of the wall. The calculated bubble sizes, based on formation dynamics, are shown in Table 2 and are based on measured values of the liquid-surface tension (Burns, 1995) for the present experiments. The surface tension for all the lowered surface-tension cases was measured to be ~ 30 dyne/cm.

Velocity measurements

Of the two traditional methods of measuring liquid velocity, hot-wire anemometry and the Pavlov tube, the latter would not work under lowered surface-tension conditions owing to the amount of surfactant used in the bubble column (sodium dodecyl sulfate, SDS, concentration ~ 1.475 mg/L and 0.05% by volume of decyl alcohol). The Pavlov tube (Figure 4b) under these lowered surface-tension conditions would trap smaller bubbles in the connecting tubing, which contaminated the pressure signals to the inclined manometer. This was because the capillary pressure of a bubble was of the same order of magnitude as the liquid-velocity head we were trying to measure. This proved to be a problem regardless of how small the holes in the Pavlov tube were constructed. On the other hand, in tap water, the Pavlov system responded well and mean axial liquid velocities could be accurately measured.

A hot-wire anemometer presents more of a problem in tap-water systems than does a Pavlov tube. Each element of the hot-wire probe (i.e, steel-clad probe) is influenced and cooled by liquid velocities and liquid-velocity fluctuations in all directions that results in a signal that must be strenusously deciphered in order to extract information about the mean liquid velocity in any of the three coordinate directions. This means generally more than one probe must be used in order to cross-correlate the signals to obtain meaningful axial liquid-velocity estimates. Furthermore, the probes are also very sensitive to small concentrations of oils and contaminants in the water that foul the probe (Buchholz and Schugerl, 1979; Hollasch and Gephart, 1972). Data acquisition is further complicated by bubbles interacting with the probes themselves (Farrar and Bruun, 1989). Introducing a relatively large amount of surfactant into the two-phase solution when the anemometer has been calibrated in tap water only complicates this difficult situation into an intractable one.

The individual problems of each measurement technique can be circumvented if the two are calibrated against one another in tap-water solutions. Then the calibration of the anemometer/steel-clad probe in the surfactant system can be used to estimate velocity, as we show. For this latter calibration, we choose to use a steel-clad probe (Figure 4c), which would withstand the rigors of two-phase flow and surface-contaminant levels, but more importantly, it had a relatively large surface area (6 mm long by 1 mm in diameter) that should reduce the effect of small bubbles impacting the probe. Unfortunately, the steel-clad probe measured both the mean velocity and velocity fluctuations in all directions. However, it allowed easy measurements on contaminated (surfactant-laced) systems.

The Pavlov tube and hot-wire anemometer/steel-clad probe were individually calibrated in the bubble column using tap water and then compared to one another. A representative comparison plot is shown in Figure 2 for center-line measurements at varying superficial gas velocities. The difference between the velocity measured by the hot-wire anemometer/steel-clad probe and the Pavlov tube represents the fluctua-

Table 2. Parameters Obtained from Indicated Data

Reference	U_{OG} cm/s	σ dyne/cm	d_B cm	d_C cm	$\bar{\epsilon}$	ϵ_C	ϵ_B	λ	δ	k	Q_C L/min	Flow Regime
Hills (1974)	1.9	72	0.59	13.79	0.070	0.090	0.052	0.981	0.725	1.13	16.25	Bubbly Flow
Hills (1974)	3.8	72	0.71	13.79	0.130	0.173	0.086	0.982	0.733	0.0230	21.03	Churn Turb
Hills (1974)	6.4	72	0.65	13.79	0.180	0.245	0.109	0.983	0.741	0.0250	24.37	Churn Turb
Hills (1974)	9.5	72	0.56	13.79	0.198	0.277	0.108	0.982	0.746	0.0250	26.30	Churn Turb
Hills (1974)	16.9	72	0.44	13.79	0.220	0.308	0.118	0.981	0.749	0.0185	32.37	Churn Turb
Devanathan et al. (1992)	10.5	72	1.50	30.61	0.180	0.235	0.117	0.990	0.744	0.0295	135.13	Churn Turb
Burns (1995)	1.25	30	0.33	13.97	0.068	0.097	0.039	0.977	0.725	3.40	20.80	Bubbly Flow
Burns (1995)	1.74	30	0.37	13.97	0.118	0.164	0.071	0.978	0.731	2.74	31.69	Bubbly Flow
Burns (1995)	2.25	30	0.40	13.97	0.146	0.201	0.089	0.980	0.736	2.77	31.04	Bubbly Flow

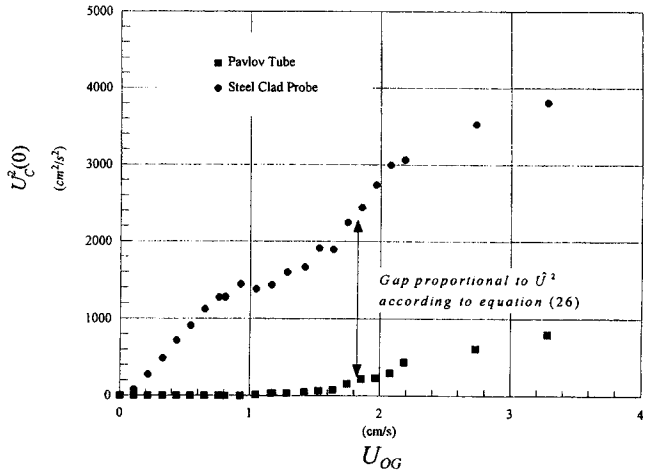

Figure 2. Velocity measured by both the hot-wire anemometer/steel-clad probe and the Pavlov tube for the center line, $\xi = 0$, of the column-for-tap, surfactan-free water.

The difference denoted by the arrow represents the fluctuation velocity owing to bubble wakes.

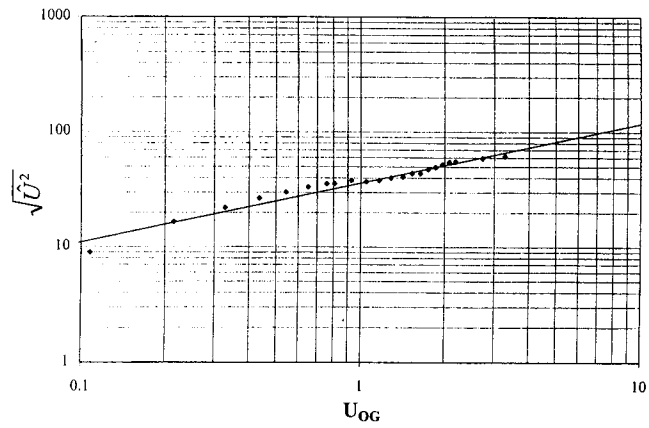

Figure 3. Turbulent-fluctuation velocity as a function of U_{OG} in the center line of the column for tap water.

tion velocity. In fact, the mean turbulent-fluctuation velocity can be taken to be the difference between the two as follows:

$$\sqrt{\hat{U}^2} = \sqrt{U_{ANE}^2 - U_{PAV}^2} \tag{26}$$

since the Pavlov tube is purely unidirectional. The variation of $\sqrt{\hat{U}^2}$ was found to be relatively independent of radial position in both coalescence-supporting and -suppressing media by Buchholz et al. (I, 1979) and Buchholz and Schugerl (II, 1979). The microturbulence scale and the bubble size may be linked, according to Rice and Geary (1990), which implies that the microturbulence fluctuations may be linearly dependent on the bubble size. Now, if the bubble size does not vary with radial position in the column, then local turbulence fluctuations should also be invariant with radial position. This can be inferred if we plot the fluctuation velocity taken from Figure 2 vs. the superficial gas velocity on a log-log scale, such as in Figure 3, where a straight line with slope 0.5 results. Bubble formation models (Rice and Geary, 1990; Geary and Rice, 1991) show this same dependence; that is, bubble size varies as the square root of the superficial gas velocity. As the gas velocity is increased and the churn-turbulent flow regime prevails, the coalescing and breakage dynamics begin to control the bubble size and bubble shape, leading to a different dependence on the gas velocity. Measurements from each probe, expressed as in Figure 2, could be used to map out the turbulent fluctuation velocity vs. gas velocity in the tap-water system. This could then be used to convert hot-wire anemometer/steel-clad probe measurements in surfactant-laced systems to an equivalent axial velocity using Figure 3 and Eq. 26. The error in $\sqrt{\hat{U}^2}$ at low liquid velocities is associated with the velocity obtained from the Pavlov tube. The manometer system used a Merium Blue manometer fluid (s.g. ~ 1.25) to pick up small variations in pressure caused by the liquid-velocity head. This system is not as accurate for low velocity as is the hot-wire anemometer. This causes some variation at the low velocities, as seen in Figure 3.

Both probes were calibrated in tap water at the radial dimensionless positions of 0.0, 03, 0.7 and 0.9 located midway up the column axis. Little variation in the fluctuation velocity ($\lesssim 10\%$) was found to exist between any of the four positions for the flow rates measured, $U_{OG} = 1.25$–2.25 cm/s. This is supported by the work of Buchholz et al. (I, 1979) and Buchholz and Schugerl (II, 1979), who also found little variation in the local turbulent fluctuation velocity with radial position. For the lowered surface tension, the bubble size could not be measured using the typical visual technique (Geary, 1992) owing to the milkiness of the emulsion. Bubbles near the wall of the milky two-phase emulsion appeared to be quite uniform. Furthermore, large transient eddies indicative of churn turbulence were not observed. This suggests that the bubbly-flow regime was realized, as expected for lowered surface-tension liquids under such conditions. The bubble size was calculated using the two-stage bubble formation/breakage model of Geary and Rice (1991), which is applicable for the bubbly-flow regime. Thus, the inadequacy of the Pavlov tube in surfactant laced systems was circumvented using the hot-wire anemometer/steel-clad probe along with the calibration curves for tap water (Figure 3).

It must be noted that the anemometer velocity measurements in the surfactant-laced system may be slightly overestimated using the tap-water calibration curves. This arises because the bubble sizes in surfactant-laced systems are smaller than for pure systems, thereby reducing the magnitude of the turbulent fluctuations. This would reduce the gap between curves in Figure 2. So the assumption that turbulent fluctuations are equivalent for the tap-water and surfactant systems may be questioned, if as we propose, the bubble size controls eddy size. This is not always the case, since eddies from wall-generated turbulence also coexist. Nonetheless, we use this velocity information to tune the current model for the surfactant-laced system. Before we can begin fitting the model, the voidage profile must first be measured.

Voidage measurements

Typically, the local voidage or gas holdup is determined using a conductance probe technique in which an insulated needle, exposed only at the tip, is immersed in a bubble field

where the liquid is conducting electric current. When the needle tip is in the water, the circuit is closed and current flows to the probe, but when a bubble impacts the probe tip and is punctured, the circuit is broken and no current flows to the probe. The exact details of this probe are published elsewhere (Serizawa et al., 1974). However, the conductance probe fails to accurately predict local voidage when the water contains large concentrations of surfactants for a number of reasons. The thick layer of charged surfactant molecules surrounding a bubble acts both as a physical barrier and an electromagnetic barrier to the needlelike conductance probe. Both the tip of the conductance probe and the charge on the bubble surface are negatively charged and tend to repel one another. Finally, the presence of the surfactant layer also makes it physically more difficult for the needle to puncture the bubble, which results in many inefficient "hits" and glances, as we observed after several attempts to use such a probe.

The isokinetic sampling method developed in this work, shown in Figure 4a, bypasses the barrier problem by continually sampling the emulsion in a flowthrough system using light attenuation to differentiate between the gas and liquid. The sample is sucked through a small capillary, 1.5 mm in diameter, which forces the bubbles into slug flow. The sampling rate is determined from the mean axial liquid-velocity profiles measured independently using the calibrated hot-wire anemometer discussed previously. The sampling rate is such that the mean axial velocity profile is not disturbed, and hence the sample is taken isokinetically (Rosner, 1986). The sampled bubble slugs pass between an infrared LED and a phototransistor. The LED and phototransistor are housed diametrically opposed to one another in a thin channel cut through two blocks of wood and are wired to a circuit board placed directly under the housing. This circuit board contains the remaining components of the electronic circuit and wiring that connects the circuit to a computer. All exposed wiring is insulated and the circuit board itself is encased in silicone sealant to protect it from water short-circuiting (Burns, 1995).

The channel connecting the two photoelectric elements intersects another channel in which the capillary is placed; this places the capillary tubing directly in between the detector and the LED. The voltage drop across the phototransistor is proportional to the amount of light it detects; consequently, the phototransistor acts as switch; a lower voltage drop is detected when the light is attenauted by liquid, switching to a higher value as gas passes by the detector–emitter pair. The time constant for the switching is equal to the time constant for the phototransistor, which is roughly on the order of a nanosecond. From this it is obvious that the time constant for the phototransistor will be far smaller than the time constant for the system. Because the signal from the phototransistor behaves much more like a square wave than does the signal from a conductance probe, it requires less data manipulation to calculate the mean local voidage.

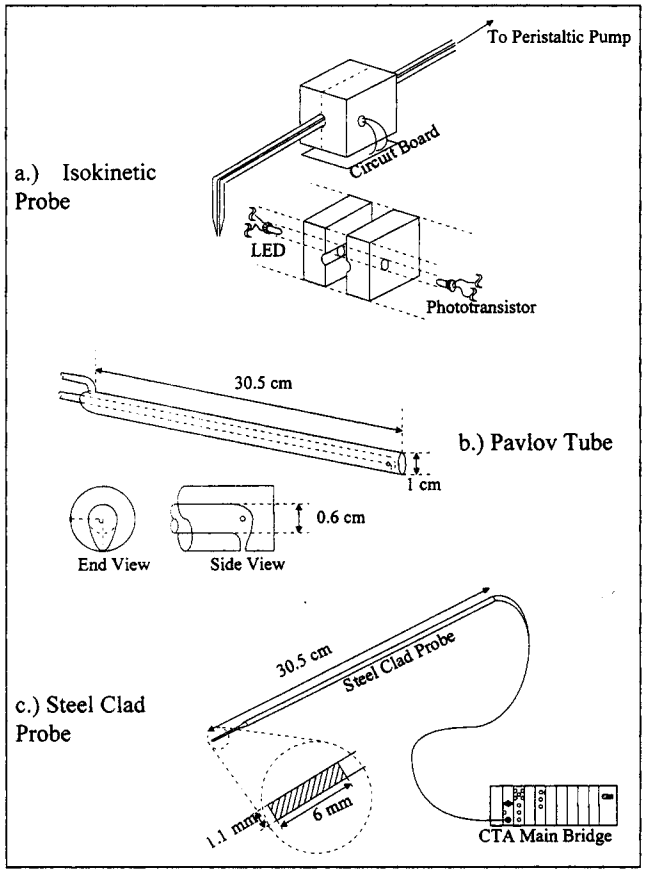

Figure 4. Isokinetic voidage sampling probe, Pavlov tube, and the hot-wire anemometer/steel-clad probe.

Experimental Details

The Pavlov tube is constructed of two tubes of glass arranged to form an annulus in which the inner tube is supported at one end by a thin capillary connecting it to the outer tube, forming the first tap or inner tap (Figure 4b). As with Hills' (1974) design, the other tap is located in the same plane as the first tap, but it is offset 90° from the inner tap. Both the inner and outer taps were made to be no larger than 1 mm in diameter, which was found to be small enough to prevent bubbles from entering the tubing in high-surface-tension fluids, such as pure water. At the opposite end of the Pavlov tube there are two glass nipples used to attach flexible tubing; these nipples are connected to an inclined manometer where the pressure difference can be measured. The clear glass walls of the Pavlov tube enabled us to quickly detect whether any bubbles had entered the tubing (Burns, 1995).

The hot-wire anemometer was a Dantec 56C17 main bridge unit with multipurpose signal conditioner, linearizer, and mean value unit. The steel-clad probe, Dantec catalog number 55R47, was connected to the unit using a 5-m coaxial cable. Details of both the steel-clad probe and the Pavlov tube are given in Figure 4. The unit was connected to a PC using Notebook for DOS to give automatic data acquisition.

The acrylic bubble column was 13.97 cm internal diameter and 240 cm in height, and is shown in Figure 5. Both the Pavlov tube and the steel-clad probe were placed 116 cm upward from the sparger of the column, although not at the same time. The sparger used in this study was a rubber-sheet sparger, otherwise known as the Flexisparger. The Flexisparger had 151 holes drilled into its face in a 7-mm triangular pitch using a #79 drill bit, which resulted in a mean hole size of 0.353 mm. The performance of this same Flexisparger

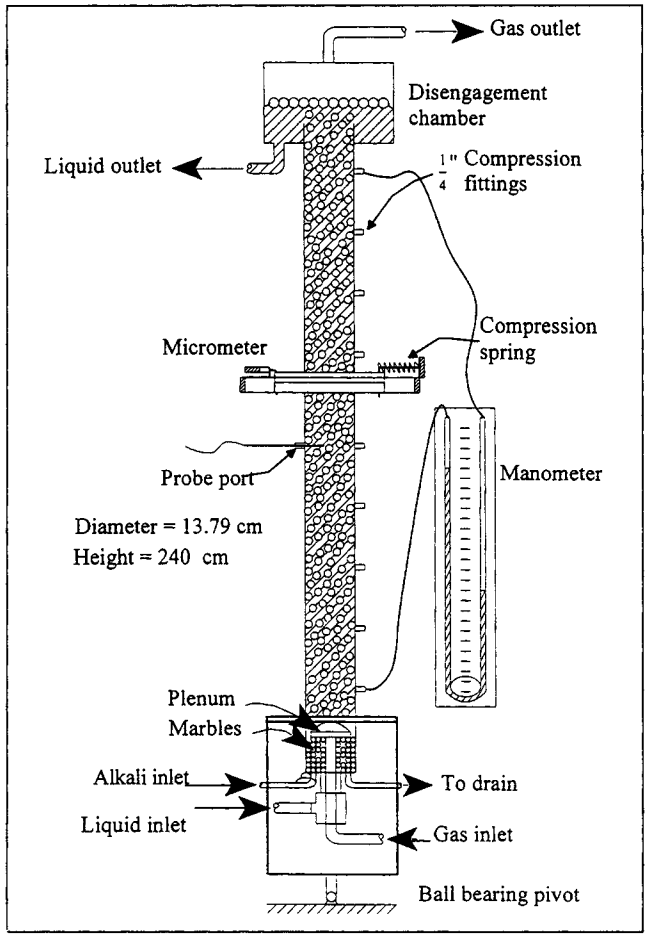

Figure 5. Bubble column.

is discussed by Geary and Rice (1991), who provide a method to calculate bubble-formation size for flexible spargers.

Experimental Results Compared with Theory

The voidage profiles for the three superficial-gas velocities chosen here, $U_{OG} = 1.25$, 1.75 and 2.25 cm/s, are given in Figure 6 along with the fitted staircase profiles. The mean values of the holdup are also shown in the figure. In all cases, the voidage profiles show a relatively flat plug shape in the central core, gradually trailing off as the wall is approached. As the wall is approached, however, the isokinetic sampling probe had difficulty in properly sampling the two-phase emulsion owing to the high velocity of downflowing water against the upflowing gas (countercurrent flow). As a result, the values near the wall are much less reliable than the ones in the central core (cocurrent flow). This problem was also reported by Hills (1974) using the conductance probe method. Errors in the buffer region voidage do not seriously affect the model calculations because the liquid-velocity prediction does not require an accurate value of the local voidage in the buffer region. The buffer zone voidage is in fact calculated using the gas-phase mass balance, Eq. 2, once estimates of the mean voidage and the core voidage are known along with calculated values of δ and λ.

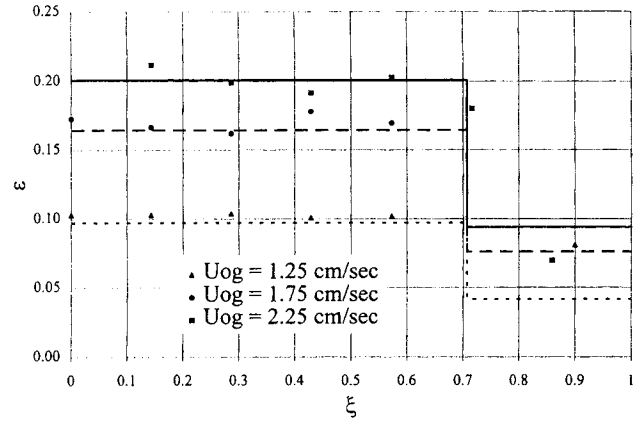

Figure 6. Voidage data from the isokinetic sampling method in lowered surface tension water.

The lines are the fitted staircase model.

Circulation velocities, inferred from anemometer measurements, were entirely in the bubbly-flow regime with values as high as 50 cm/s at the center line (Burns, 1995). Figure 7 shows data and theory for the liquid circulation velocity profiles at superficial gas velocities of 1.25 and 2.25 cm/s, both of which are well within the bubbly-flow regime. Only two model curves are illustrated to prevent clutter. Results for the case $U_{OG} = 1.75$ cm/s are presented in Figure 8 and Table 2, where parameters are provided for all cases considered. As with the literature data, we see a definitive plug shape to the measured velocity profile in the center of the column as well as with the tuned model. For the lowered surface tension data, we have already shown that the proper length scale is probably the bubble size and not the column diameter. Therefore, the column diameter in Eqs. 15 and 17 can be replaced with the bubble diameter. In this case, the calculated values of k are roughly two orders of magnitude greater than those calculated using the column diameter. The k values were also slightly higher than for the bubbly-flow data reported by Hills ($U_{OG} = 1.9$ cm/s yielding a $k = 1.13$), as we discuss in the next section. This discrepancy is attributed to the uncertainty in the calculated bubble diameters, since bubble sizes were not provided by Hills. The average value of k for all bubbly-flow data was 2.51, thus the

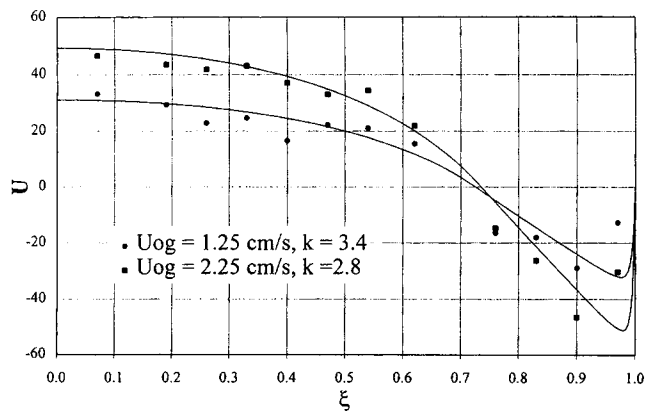

Figure 7. Lowered surface tension data vs. fitted model for U_{OG} of 1.25 and 2.25 cm/s.

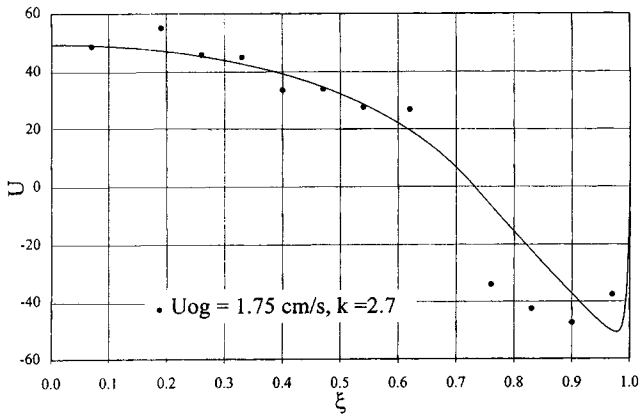

Figure 8. Lowered surface tension data vs. fitted model for U_{OG} of 1.75 cm/s.

integral average for ν_t is: $(\nu_t)_{avg} = 1.08 d_B^{4/3}(U_{OG}g)^{1/3}$, which is almost identical with the dispersion results of Rice and Littlefeld (1987), namely $D_e = d_B^{4/3}(U_{OG}g)^{1/3}$.

Literature Data Compared with Theory

When testing liquid velocity predicted by theory (Eqs. 18–20) against experimental data, specific and detailed information about the system of study is needed in order to completely define the hydrodynamics. It is for this reason that the data of Hills (1974) are often chosen as a benchmark to test liquid-velocity prediction profiles. Hills provided detailed information on the sparger specifics, column dimensions, water conditions, and most importantly, the radial voidage profiles. The voidage profiles of Hills are given in Figure 9 and the fitted (average) values of the voidage in the core and the buffer region are reported in Table 2. To initiate the search for δ and λ, initial values are taken as roughly 0.707 and 1.0, respectively, which corresponds to equal areas of upflow and downflow. Subsequent calculations show later that the values of δ and λ do not diverge greatly from these initial values. Small deviations in either δ and λ should not affect the regressed values of the voidage in either the core or buffer regions owing to the discrete nature of the data.

For the flow rates shown in Table 2, Hills voidage data showed a relatively flat profile in the core region decreasing as the wall is approached, which bears a striking resemblance to the square-wave profile portrayed in Figure 1. However, near the wall, the model does a poor job of describing the local voidage profile where experimental errors were large according to Hills. This poor quality of the data will have little effect on the predicted values, because the buffer-region voidage is inferred from the gas-phase mass balance (Eq. 2), which depends on the core region and overall voidage. Both of these are more accurately measured than voidage near the wall. Consequently, the model circumvents experimental error in voidage measurements near the wall by relying on accurate data obtained elsewhere in the column.

The velocity profiles shown in Figure 10 were calculated first by estimating the values of the voidage profile in the core and the mean voidage as reported by Hills. To start the routine, a value of the proportionality constant, k, is chosen. The values of the inversion point, δ, the point of maximum downflow λ, and the voidage in the buffer region, ϵ_B, are then solved numerically by invoking Eqs. 2, 22 and 25. The integrals were evaluated using a 16-point Gaussian quadrature, and the equations were solved numerically using the well-established Newton-Raphson root-solving technique. The velocity profile was then visually compared against the reported experimental data for goodness of fit and a sum of the residuals was calculated. An adjustment in k was then made, and the routine was repeated until a satisfactory visual fit resulted (i.e., when the residuals were minimized).

In the case of Hills data, only one data set fell within the bubbly flow regime ($U_{OG} = 1.9$ cm/s). For this data set, the column diameter in Eqs. 15 and 17 was replaced with the calculated bubble diameter (see Table 2). The fit of the calculated velocity profile very closely simulates the "pluglike" shape of the data reported by Hills. This differs from literature models, which have shown a more parabolic form. Pluglike behavior has been observed by many different authors, even at high gas throughputs. Devanathan et al. (1990) reported liquid-velocity data for superficial-gas velocities of 10.5 cm/s (well beyond the bubbly-flow regime) using particle-tracking technology. Even at these high velocities the shape of the liquid-velocity profile in the center gave a plug shape,

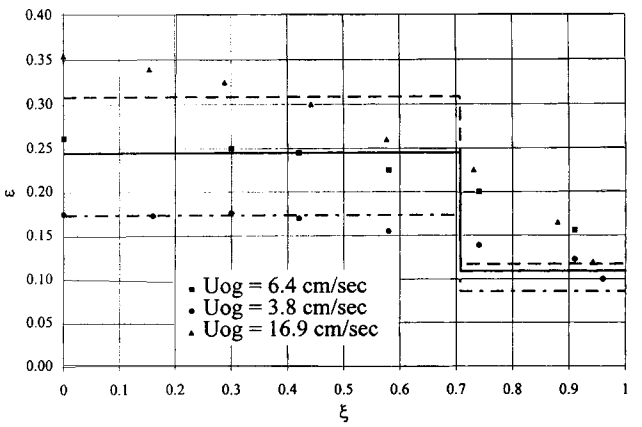

Figure 9. Hills' (1974) voidage data for varying U_{OG} (details in Table 2).

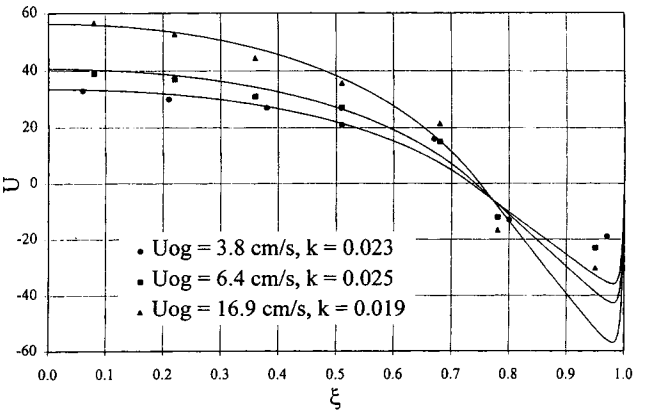

Figure 10. Hills' (1974) velocity data vs. fitted model for U_{OG} of 3.8, 6.4, and 16.9 cm/s (details in Table 2).

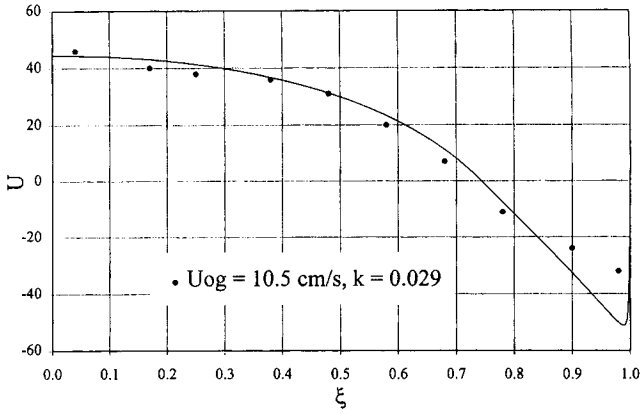

Figure 11. Devananthan et al. (1990) data vs. fitted model for U_{OG} of 10.5 cm/s (details in Table 2).

as can be seen in Figure 11. In the case of Devanathan's data, some important details of the experimental setup were left out of the original work, namely the sparger specifications and the radial voidage profile. The voidage profile for Devanathan's work was estimated using data obtained by Geary and Rice (1992), who fitted the value of m in the voidage profile (Eq. 1) to Devanathan's data; that is, they used reported values of the mean voidage to estimate m in Eq. 1, which was found to be equal to 6. Equation 1 was then averaged from 0 to δ to yield a value for the core voidage. The mean voidage was also given so that Eq. 2 was used.

The tuned values of k and the numerically determined values of δ, λ, and ϵ_B are given in Table 2. For the churn-turbulent data of Hills, the tuned parameter k varies only slightly around a mean value. When the model was tuned to the data of Devanathan, the value of k was found to be slightly larger.

Comments and Conclusions

We have presented a liquid-circulation prediction theory based on an energy-dissipation model for turbulent (eddy) viscosity. The liquid-circulation model is dependent on a single proportionality constant, which was tuned to both literature and new lowered surface-tension liquid-velocity data in the bubbly-flow and churn-turbulent flow regimes. The length scales for turbulent mixing were taken to be equal to the bubble diameter for bubbly flow and the column diameter for churn turbulence. This yielded two sets of tuned values for the proportionality constant, which yielded two tuned average values: $k \approx 2.51$ (bubbly flow) and $k \approx 0.0242$ (churn turbulence). The results for the bubbly flow suggest $(\nu_t)_{\text{avg}} \approx D_e$ within experimental error. The energy-dissipation model for turbulent viscosity affects the shape of the liquid-velocity profile, which we showed should be more plug shaped in the center of the column rather than the conventional parabolic shape often seen in the literature.

Important new methods for measuring both the liquid velocity and the local voidage in a bubble column have been presented. These methods were developed because traditional techniques used to measure these parameters failed in surfactant-laced systems. The methods seem to have wide applicability in a multitude of different low-surface-tension multiphase bubble columns. We also argue that a complete voidage profile is probably not necessary for accurate velocity predictions. The simplified staircase function requires only two values of the voidage: the mean value in the central core and the overall mean in the column. This simplifies the experiments needed for designing and modeling bubble columns.

Finally, we remark again that intense liquid circulation was spontaneously induced by adding small amounts of surfactant, sodium dodecyl sulfate, and decyl alcohol. It is thought to be a result of the surfactant layer transforming the bubble into a more spherical shape by reducing its size and at the same time making the bubble more rigid. This well-known effect could cause the bubble to behave more as a rigid sphere than a bubble. If this were the case, the bubble in the presence of a velocity field could begin to spin, wherein the bubble would generate a lateral force known as the Magnus force. This is the same force that enables a pitcher to throw a curve ball in a baseball game. The spin owing to an imposed velocity gradient would cause the bubbles to move toward the center of the column (Drew, 1988; Drew et al., 1991), forming a gradient in the radial-gas holdup, which further stimulates the full development of buoyancy-driven flow. Low-surface-tension systems are widely used in the process industries, including coal liquefaction slurries, fermentation processes, and flotation systems. The current research suggests that strong circulation is likely to arise for these processes.

Acknowledgments

We are grateful to the Exxon Research and Development Laboratories and Louisiana Education Quality Support Fund (LEQSF) for funding this project.

Notation

A = cross-sectional area of the column, cm^2
D_e = eddy dispersion coefficient, cm^2/s
g = gravitational constant, cm/s^2
p = pressure, atm
r = variable radial coordinate, cm
R = column radius, cm
R_C = Reynolds stress for continuous phase, dyne/cm^2
$\bar{T}$ = the total stress tensor in the continuous phase, dyne/cm^3
U = local liquid velocity, cm/s
U_{og} = superficial-gas velocity, cm/s
U_{OL} = superficial-liquid velocity, cm/s
U_S = slip velocity, cm/s
V = dispersed-phase velocity, cm/s
δ = dimensionless inversion point
λ = dimensionless position of maximum downflow
μ_L = liquid viscosity, poise
μ_t = turbulent viscosity, poise
ν_L = liquid kinematic viscosity, cm^2/s
ρ_g = gas density, g/cm^3
ρ_L = liquid density, g/cm^3
σ = surface tension, dyne/cm

Literature Cited

Anderson, K. G., and R. G. Rice, "Local Turbulence Model for Predicting Circulation Rates in Bubble Columns," *AIChE J.*, **35**, 514 (1989).
Baird, M. H. I., and R. G. Rice, "Axial Dispersion in Large Unbaffled Bubble Columns," *Chem. Eng. J.*, **9**, 171 (1975).
Bird, R. B., W. E. Stewart, and E. N. Lightfoot, *Transport Phenomena*, Wiley, New York (1960).
Buchholz, R., I. Alder, and K. Schugerl, "Investigation of the Struc-

ture of Two-Phase Flow Model-Media in Bubble Column Bioreactors: II. Transverse Variation of Local Properties when Coalescence Suppressing Media Are Used," *Eur. J. Appl. Microbiol. Biotech.*, **7**, 241 (1979).
Buchholz, R., I. Alder, and K. Schugerl, "Investigation of the Structure of Two-Phase Flow Model-Media in Bubble Column Bioreactors: I. Transverse Variation of Local Properties when Coalescence Promoting Media are used," *Eur. J. Appl. Microbiol. Biotech.*, **7**, 135 (1979).
Buchholz, R., and K. Schugerl, "Methods for Measuring the Properties of the Turbulence in Bubbly Flow," *Eur. J. Appl. Microbiol. Biotech.*, **7**, 11 (1979).
Burns, L. F., *The Effect of Lowered Surface Tension on Fluid Dynamics and Mass Transfer in Bubble Column Reactors*, MS Thesis, Louisiana State University, Baton Rouge (1995).
Deckwer, W. D., G. Zoll, R. Burckhart, and Y. T. Shah, "Mixing and Mass Transfer in Tall Bubble Columns," *Chem. Eng. Sci.*, **29**, 2177 (1974).
Devanathan, N., M. P. Dudukovic, A. Lapin, and A. Lubbert, "Chaotic Flow in Bubble Column Reactors," *Chem. Eng. Sci.*, **50**, 2661 (1995).
Devanathan, N., D. Moslemian, and M. P. Dudukovic, "Flow Mapping in Bubble Columns using CARPT," *Chem. Eng. Sci.*, **45**, 2285 (1990).
Drew, D. A., "The Lift Force on a Small Sphere in the Presence of a Wall," *Chem. Eng. Sci.*, **43**, 769 (1988).
Drew, D. A., J. A. Schonberg, and G. Belfort, "Lateral Inertial Migration of a Small Sphere in Fast Laminar Flow Through a Membrane Duct," *Chem. Eng. Sci.*, **46**, 3219 (1991).
Farrar, B., and H. Brunn, "Interaction Effects Between a Cylindrical Hot-Film Anemometer Probe and Bubbles in Air/Water and Oil/Water Flows," *J. Phys. Eng. Sci. Instrum.*, **22**, 114 (1989).
Geary, N. W., "On Bubble Columns," PhD Diss., Louisiana State Univ., Baton Rouge (1992).
Geary, N. W., and R. G. Rice, "Bubble Size Prediction for Rigid and Flexible Spargers," *AIChE J.*, **37**, 161 (1991).
Geary, N. W., and R. G. Rice, "Circulation and Scale up in Bubble Columns," *AIChE J.*, **38**, 76 (1992).
Grienberger, J., and H. Hofmann, "Investigations and Modelling of Bubble Columns," *Chem. Eng. Sci.*, **47**, 2215 (1992).
Hills, J. H., "Operation of a Bubble Column at High Throughputs: I. Gas Hold up Measurements," *Chem. Eng. J.*, **12**, 89 (1976).
Hills, J. H., "Radial Non-uniformity of Velocity and Voidage in a Bubble Column," *Trans. Inst. Chem. Eng.*, **52**, 1 (1974).
Hollasch, K., and B. Gephart, "Calibration of Constant-temperature Hot-wire Anemometers at Low Velocities in Water with Variable Fluid Temperature," *J. Heat Transfer*, **12**, 17 (1972).
Ishii, M., and N. Zuber, "Drag Coefficient and Relative Velocity in Bubbly, Droplet, or Particulate Flows," *AIChE J.*, **25**, 843 (1979).
Ishii, M., *Thermo-Fluid Dynamic Theory of Two-Phase Flow*, Eyrolles, Paris (1975).
Knudsen, J. G., and D. L. Katz, *Fluid Dynamics and Heat Transfer*, McGraw-Hill, New York (1958).
Luo, H., and H. F. Svendsen, "Turbulent Circulation in Bubble Columns from Eddy Viscosity Distributions of Single Phase Pipe Flow," *Can. J. Chem. Eng.*, **69**, 1389 (1991).
Menzel, T., T. in der Weide, O. Staudacher, O. Wein, and U. Onken, "Reynolds Shear Stress for Modelling of Bubble Column Reactors," *Ind. Eng. Chem. Res.*, **29**, 988 (1990).
Rice, R. G., D. T. Barbe, and N. W. Geary, "Correlation of Nonverticality and Entrance Effects in Bubble Columns," *AIChE J.*, **36**, 1421 (1990).
Rice, R. G., and N. W. Geary, "Prediction of Liquid Circulation in Viscous Bubble Columns," *AIChE J.*, **36**, 1339 (1990).
Rice, R. G., N. W. Geary, and L. F. Burns, "Circulation Model for Absorption and Dispersion in Cocurrent Bubble Columns," *AIChE E.*, **39**, 224 (1993).
Rice, R. G., and M. A. Littlefield, "Dispersion Coefficients for Ideal Bubbly Flow in Truly Vertical Bubble Columns," *Chem. Eng. Sci.*, **42**, 2045 (1987).
Rietema, K., "Science and Technology of Dispersed Two-Phase Systems—I and II," *Chem. Eng. Sci.*, **37**, 1125 (1982).
Rietema, K., and S. P. P. Ottengraf, "Laminar Liquid Circulation and Bubble Street Formation in a Gas-Liquid-System," *Trans. Inst. Chem. Eng.*, **48**, T54 (1970).
Rosner, D. E., *Transport Processes in Chemically Reacting Flow Systems*, Butterworth, Stoneham, MA (1986).
Serizawa, A., I. Kataoka, and I. Michioyshi, "Turbulence Structure of Air-Water Bubbly Flow: I. Measuring Techniques," *Int. J. Multiphase Flow*, **2**, 221 (1974).
ibid.: "II. Local Properties," **2**, 234 (1974).
ibid.: "III. Transport Properties," **2**, 247 (1974).
Shah, Y. T., B. G. Kelkar, S. P. Godbole, and W. D. Deckwer, "Design Parameters Estimations for Bubble Column Reactors," *AIChE J.*, **28**, 353 (1982).
Ueyama, K., and T. Miyauchi, "Properties of Recirculating Turbulent Two Phase Flow in Gas Bubble Columns," *AIChE J.*, **25**, 258 (1979).
Ulbrecht, J. J., and Z. S. Baykara, "Significance of the Central Plume Velocity for the Correlation of Liquid Phase Mixing in Bubble Columns," *Chem. Eng. Commun.*, **10**, 165 (1981).
Wallis, G. B., *One-Dimensional Two-Phase Flow*, McGraw-Hill, New York (1969).

Appendix

For the assumed profile given by $n = 2$, an analytic solution for the velocity profile can be written as a function of two integrals:

$$I_1(\xi) = -\frac{2}{3}\int \frac{\xi}{(1-\xi^2)^{4/3}+\alpha}\,d\xi = \int \frac{q^2}{q^4+\alpha}\,dq \tag{A1}$$

and

$$I_2(\xi) = -\frac{2}{3}\int \frac{1}{(1-\xi^2)^{4/3}+\alpha}\,\frac{d\xi}{\xi} = \int \frac{q^2}{(q^4+\alpha)(1-q^3)}\,dq, \tag{A2}$$

where

$$q(\xi) = (1-\xi^2)^{1/3}. \tag{A3}$$

Both integrals have analytic solutions. They are written as

$$I_1(\xi) = \frac{\sqrt{2}}{8\alpha^{1/4}}\left\{\ln\left(\frac{\phi(\xi)\psi(\xi)+1-2\phi(\xi)}{\phi(\xi)\psi(\xi)+1+2\psi(\xi)}\right) + 2\arctan[\psi(\xi)] + 2\arctan[\phi(\xi)]\right\} \tag{A4}$$

and

$$I_2(\xi)=\frac{\alpha^2}{4(1+\alpha^3)}\ln[q^4(\xi)+\alpha]-\frac{1}{3(1+\alpha)}\ln[1-q(\xi)]$$
$$-\frac{\sqrt{3}}{3(\alpha^2-\alpha+1)}\arctan\left\{\frac{\sqrt{3}}{3}[1+2q(\xi)]\right\}$$
$$+\frac{1-2\alpha}{6(\alpha^2-\alpha+1)}\ln[q^2(\xi)+q(\xi)+1]$$
$$-\frac{\sqrt{\alpha}}{2(1+\alpha^3)}\arctan\left[\frac{\phi(\xi)\psi(\xi)+1}{2}\right]$$
$$+\frac{\sqrt{2}\,(1-\alpha^{3/2})}{8\alpha^{1/4}(1+\alpha^3)}\ln\left[\frac{\phi(\xi)\psi(\xi)+1-2\phi(\xi)}{\phi(\xi)\psi(\xi)+1+2\psi(\xi)}\right]$$
$$+\frac{\sqrt{2}\,(1+\alpha^{3/2})}{4\alpha^{1/4}(1+\alpha^3)}\{\arctan[\phi(\xi)]+\arctan[\psi(\xi)]\},\quad\text{(A5)}$$

where

$$\phi(\xi)=\frac{\sqrt{2}\,q(\xi)}{\alpha^{1/4}}-1\quad\text{(A6)}$$

and

$$\psi(\xi)=\frac{\sqrt{2}\,q(\xi)}{\alpha^{1/4}}+1.\quad\text{(A7)}$$

The solutions to the velocity profile in each of the three regions are algebraic functions of I_1 and I_2. The core region velocity profile is then given by the relation:

$$U_C(\xi)=\frac{3\alpha\beta_C}{2}[I_1(\xi)-I_1(\delta)].\quad\text{(A8)}$$

Similarly, the buffer and wall region velocity profiles are then, respectively,

$$U_B(\xi)=U_W(\lambda)+\frac{3\alpha\beta_B}{2}\{\lambda^2[I_2(\xi)-I_2(\lambda)]-I_1(\xi)+I_1(\lambda)\},\quad\text{(A9)}$$

$$U_W(\xi)=\frac{3\alpha\beta_W}{2}\{\lambda^2[I_2(\xi)-I_2(1)]-I_1(\xi)+I_1(1)\}.\quad\text{(A10)}$$

Manuscript received May 31, 1996, and revision received Feb. 7, 1997.